
Article:
Giarè, W. orcid.org/0000-0002-4012-9285, Mena, O. orcid.org/0000-0001-5225-975X and Di Valentino, E. orcid.org/0000-0001-8408-6961 (2023) Lensing impact on cosmic relics and tensions. Physical Review D, 108 (10). 103539. ISSN 2470-0010

https://doi.org/10.1103/physrevd.108.103539

Lensing impact on cosmic relics and tensions

William Giarè,[1,*] Olga Mena,[2,†] and Eleonora Di Valentino[3,‡]

[1]*Consortium for Fundamental Physics, School of Mathematics and Statistics, University of Sheffield, Hounsfield Road, Sheffield S3 7RH, United Kingdom*

[2]*Instituto de Física Corpuscular (CSIC-Universitat de València), E-46980 Paterna, Spain*

[3]*School of Mathematics and Statistics, University of Sheffield, Hounsfield Road, Sheffield S3 7RH, United Kingdom*

(Received 3 August 2023; accepted 4 November 2023; published 28 November 2023)

Cosmological bounds on neutrinos and additional hypothetical light thermal relics, such as QCD axions, are currently among the most restrictive ones. These limits mainly rely on cosmic microwave background temperature anisotropies. Nonetheless, one of the largest cosmological signatures of thermal relics is that on gravitational lensing, due to their free-streaming behavior before their nonrelativistic period. We investigate late-time only hot-relic mass constraints, primarily based on recently released lensing data from the Atacama Cosmology Telescope, both alone and in combination with lensing data from the Planck satellite. Additionally, we consider other local probes, such as baryon acoustic oscillations measurements, shear-shear, galaxy-galaxy, and galaxy-shear correlation functions from the dark energy survey, and distance moduli measurements from Type-Ia Supernovae. The tightest bounds we find are $\sum m_\nu < 0.43$ eV and $m_a < 1.1$ eV, both at 95% CL Interestingly, these limits are still much stronger than those found on e.g., laboratory neutrino mass searches, reassessing the robustness of the extraction of thermal relic properties via cosmological observations. In addition, when considering lensing-only data, the significance of the Hubble constant tension is considerably reduced, while the clustering parameter σ_8 controversy is completely absent.

DOI: 10.1103/PhysRevD.108.103539

I. INTRODUCTION

In the standard ΛCDM cosmological model, the three flavors of light active neutrinos, as predicted within the framework of the Standard Model (SM) of elementary particles, contribute to the overall energy density of the Universe as hot thermal relics. However, theoretical attempts to address the deficiencies of the SM of particle physics often introduce additional light and elusive degrees of freedom, leading to a range of new particle candidates for physics beyond the standard model that often exhibit behaviors similar to neutrinos and can also contribute to the overall energy density as thermal relics.

Among these candidates, the QCD axion [1–4] has gained significant attention in the quest for physics beyond the SM due to its potential implications for the cosmological energy budget and its role in addressing fundamental puzzles in particle physics [5–10]. Axions can be abundantly produced in the early Universe through a wide range of physical mechanisms [11–31] and the implications of a cosmic axion background depend on the specific production mechanism employed, see e.g., Ref. [32] for a recent review. If axions are thermally produced through scatterings and particle decays within the primordial bath, they contribute to the radiation energy density, similar to massive neutrinos, and can be classified as a component of hot dark matter [23–31,33–44].

Cosmology can set very strong bounds on hot dark matter relics, including standard neutrinos [45–47] and the hypothesized thermal axions [48–52]. As for neutrinos, cosmological observations currently provide the tightest limit on the total neutrino mass, $\sum m_\nu < 0.09$ eV at 95% CL [45–47]. This constraint is comparable to the inverted-ordering lower bound ($\sum m_\nu > 0.0997 \pm 0.00051$ eV) derived from neutrino-oscillation data [53–55]. Concerning axions, the most constraining bound in the literature in a mixed hot dark matter cosmology is $m_a \lesssim 0.2$ eV, together with limits on the neutrino sector of $\Delta N_{\rm eff} < 0.23$ and $\sum m_\nu < 0.16$ eV, all at 95% CL [48–52].

All the limits above mainly rely on early Universe observations such as the Planck cosmic microwave background (CMB) data or big bang nucleosynthesis (BBN)

*w.giare@sheffield.ac.uk
†omena@ific.uv.es
‡e.divalentino@sheffield.ac.uk

measurements. Indeed it is well-known that thermal relics play a non-negligible role both during the BBN epoch and in the CMB temperature anisotropies. For instance, during the decoupling epoch, light neutrinos can transit from a relativistic to a nonrelativistic regime, thereby impacting the gravitational potentials and leaving characteristic signatures in the angular power spectra of temperature and polarization anisotropies through the integrated Sachs-Wolfe (ISW) effect, depending this imprint on the total neutrino mass $\sum m_\nu$. However, this effect, as well as the horizontal shift towards larger angular scales induced in the CMB temperature anisotropies, is largely degenerate with other cosmological parameters, as, for instance, the Hubble constant H_0 [56–58]. When substituting Planck data with a combined analysis of other independent CMB measurements provided by WMAP, ACT, and SPT-3G, the previously mentioned constraints are generally relaxed [59–61]. In certain cases, the neutrino mass bounds exceed the eV limit[1] and even show a slight preference for a larger neutrino mass value [63]. This underscores the importance of obtaining complementary constraints on thermal relics that are independent of CMB anisotropies, as they can serve as a valuable source for cross-validation.[2]

In this regard, Planck observations opened up a new era in which the dominant effect of neutrinos is due to gravitational lensing [71]. After decoupling from the thermal bath, neutrinos travel without interactions along geodesics as hot thermal relics with significant velocity dispersions. The nonrelativistic neutrino overdensities only cluster at wavelengths larger than their free-streaming scale, hindering the growth of matter fluctuations on small scales and suppressing galaxy clustering and leaving a distinct imprint on the lensing potential, especially on scales smaller than the horizon when they become nonrelativistic. Increasing neutrino masses will increase the expansion rate at $z \gtrsim 1$, suppressing clustering on scales smaller than the horizon size at the nonrelativistic transition [72,73]. This translates into a suppression of the CMB lensing power spectrum of 10% at multipoles $\ell = 1000$, assuming the minimum neutrino mass indicated by neutrino oscillation experiments, i.e., $\sum m_\nu < 0.06$ eV [71].

The former significant impact of thermal relics in the late Universe, corroborated by the significant improvement in the constraints on their properties that are achieved exploiting observations of the local Universe, suggests that ongoing advancements in reconstructing the dark matter distribution, particularly through the lensing spectrum, combined with other precise cosmological observations in the late-time Universe, may offer a promising approach to constrain thermal relics based solely on their indirect effects at later times. In this regard, the recent data Release 6 (DR6) from the Atacama Cosmology Telescope [74,75] has provided a comprehensive reconstruction of cosmic microwave background lensing over 9400 sq. deg. of the sky, opening up new avenues for studying the properties of neutrinos and other light particles.[3]

In this work, we aim to examine the constraints that can be obtained on thermal relics solely from observations of the local Universe, particularly focusing on the impact derived from recent lensing measurements in combination with other large-scale structure data. The paper is structured as follows: In Sec. II, we will describe the methodology used in our data analysis. In Sec. III, we present the main results, distinguishing between three possible scenarios. We begin by studying the simplest and most typical case where all thermal relics are represented by massive neutrinos only (see Sec. III A). Next, we fix the neutrino mass to the reference value of $\sum m_\nu \sim 0.06$ eV and analyze the constraints that can be achieved on thermal axions (Sec. III B). Finally, we perform a full joint analysis of axions and neutrinos (see Sec. III C). In Sec. IV we draw our conclusions.

II. NUMERICAL METHODOLOGY

A. Thermal relics implementation

We investigate the effects of relic populations of neutrinos and thermal axions at late cosmic times by employing a modified version of the Boltzmann integrator code CAMB [76,77]. Our tailored modifications comprehensively consider the effects of QCD axions across various cosmological scales and epochs by incorporating the axion mass as an additional cosmological parameter, similarly to massive neutrinos.[4]

Specifically, our code allows us to disentangle the distinct effects of QCD axions during early and late cosmic times. In the early Universe, when the axion is relativistic, it behaves as radiation and contributes to the effective number of neutrino species $N_{\rm eff}$. To accurately compute this contribution, we solve the Boltzmann equation for the axion number density, specifically focusing on the Kim-Shifman-Vainshtein-Zakharov (KSVZ) model of axion-hadron interactions [81,82]. While the axion is relativistic,

[1]Notice however that it can be brought down to $\sum m_\nu \lesssim 0.2$ eV when including large-scale structure information [62].

[2]This discrepancy present in the total neutrino mass constraints has been investigated for several extensions of the ΛCDM model, revealing a CMB tension between Planck and ACT [61,64–70].

[3]Remarkably, when combined with Planck CMB anisotropies data and baryon acoustic oscillation measurements, this dataset yields an upper bound of $\sum m_\nu < 0.12$ eV. This upper bound remains unchanged even when incorporating the Planck satellite lensing data.

[4]It is important to note that our code has been extensively tested in previous studies and is built upon a strong understanding of thermal axions across the QCD phase transition [43,44]. In addition, our previous results have been verified to match those obtained by independent groups using different numerical methodologies (see for instance Refs. [50–52,78–80]). We refer to Ref. [50] for a detailed step-by-step explanation of all the modifications involved.

it directly impacts the CMB angular power spectra through the early integrated Sachs-Wolfe effect, similar to massive neutrinos. Additionally, it indirectly modifies the primordial helium abundance during BBN. However, since our analysis does not incorporate observations of the early Universe, these effects have minimal impact on our results, except for their potential indirect influence on the lensing spectrum.

On the other hand, as the axion switches to a nonrelativistic regime, it behaves as cold dark matter, leading a significant influence on the process of structure formation. Notably, depending on the value of its mass, the axion may become nonrelativistic much earlier than massive neutrinos. This characteristic enables us to distinguish between the effects left by massive neutrinos and massive axions on structure formation,[5] thereby offering us the opportunity to derive joint constraints on thermal relics solely through the analysis of the lensing potential reconstruction and large-scale structure data.

B. Markov Chain Monte Carlo analysis

In order to derive observational constraints on hot thermal relics from late-time data, we perform Markov Chain Monte Carlo (MCMC) analyses using the publicly available version of the sampler `COBAYA` [83]. As our primary focus is on lensing measurements in combination with other late times observations, we use the identical setup and assumptions employed by the ACT Collaboration in their lensing Data Release 6 paper on cosmological parameters, Ref. [74]. Specifically, we adopt the same likelihoods setup discussed in Appendix A of Ref. [74], considering a fiducial cosmological model that extends the ΛCDM model to include hot relics such as neutrinos and/or axions. To ensure a direct comparison of our results with those obtained by the ACT Collaboration, we also adopt the same priors on the standard cosmological parameters, as presented in Table 1 of Ref. [74], where the CMB anisotropies data are excluded. We summarize these priors in Table I.

The convergence of the chains obtained with this procedure is tested using the Gelman-Rubin criterion [84], and we choose as a threshold for chain convergence $R-1\lesssim 0.02$.

TABLE I. Prior distributions adopted for cosmological parameters. Uniform priors are shown in square brackets and Gaussian priors with mean μ and standard deviation σ are shown as $\mathcal{N}(\mu,\sigma)$.

Parameter	Prior
$\Omega_c h^2$	[0.005, 0.99]
$\Omega_b h^2$	$\mathcal{N}(0.02233, 0.00036)$
$100\theta_{MC}$	[0.5, 10]
$\log(10^{10}A_S)$	[1.61, 4]
n_s	$\mathcal{N}(0.96, 0.02)$
$\sum m_\nu$ [eV]	[0.06, 5]
m_a [eV]	[0.01, 10]

C. Datasets

The reference datasets exploited in our analysis are given as follows:

(i) The gravitational lensing mass map covering 9400 deg^2 reconstructed from measurements of the cosmic microwave background made by the Atacama Cosmology Telescope from 2017 to 2021 [74,75]. In our analysis we include only the conservative range of lensing multipoles $40<\ell<763$. This dataset is referred to as *ACT-DR6*.

(ii) The ACT-DR6 dataset is considered both independently and in conjunction with the *Planck-2018* lensing likelihood [85], derived from the temperature 4-point correlation function. We shall refer to the combined likelihood which includes data from both ACT-DR6 and *Planck-2018* lensing simply as *full lensing*.

Additionally, we investigate a wide array of local probes of the Universe by combining these two datasets with other late-time observations, including:

(i) Baryon acoustic oscillations (BAO) and redshift space distortions (RSD) measurements obtained from a combination of the spectroscopic galaxy and quasar catalogs of the Sloan Digital Sky Survey (SDSS) [86] and the more recent eBOSS DR16 data [87,88]. To remain conservative, we exclude Quasars and Lyman-α BAO measurements from this dataset. This likelihood is referred to as *BAO*.

(ii) The Pantheon catalog which includes a collection of 1048 B-band observations of the relative magnitudes of Type-Ia supernovae [89]. This dataset is referred to as *SN*.

(iii) The shear-shear, galaxy-galaxy, and galaxy-shear correlation functions from the first year of the Dark Energy Survey [90]. We refer to this dataset as *DES*.

III. RESULTS

A. Constraints on neutrinos

The main results are summarized in Table II and III and depicted in Fig. 1.

Table II contains as the basic dataset the ACT-DR6 lensing one. Notice that the cosmological constraints by this data set alone are very poor, but nevertheless we show them for completeness. When BAO measurements are included, a 95% CL upper bound on the total neutrino mass of 1.10 eV is achieved. This result is very remarkable,

[5]Nonetheless, when the masses of axions and neutrinos are similar, the evolution of their energy densities hinders our ability to constrain their masses to values below ∼0.1 eV, as discussed in Refs. [49,50].

TABLE II. *Neutrinos:* Mean values for some of the most relevant cosmological parameters in this study, together with their 68% (95%) CL errors for the some of the possible data combinations here considered, based on the baseline ACT-DR6 lensing dataset. Upper bounds are quoted at 95% CL significance.

Parameter	ACT-DR6	ACT-DR6 + BAO	ACT-DR6 + BAO + DES	ACT-DR6 + BAO + SN	ACT-DR6 + BAO + DES + SN
$\sum m_\nu$[eV]	<3.32	<1.10	<0.773	<0.717	<0.722
$\Omega_{\rm m}$	$1.27^{+0.79}_{-1.6}(<3.90)$	$0.344^{+0.031}_{-0.035}(0.344^{+0.067}_{-0.063})$	$0.303 \pm 0.014(0.303^{+0.030}_{-0.029})$	$0.316 \pm 0.016(0.316^{+0.035}_{-0.034})$	$0.302 \pm 0.012(0.302^{+0.023}_{-0.021})$
H_0	<58.8 (unc)	$68.7 \pm 1.4(68.7^{+3.0}_{-2.9})$	$67.21 \pm 0.87(67.2^{+1.8}_{-1.7})$	$67.9 \pm 1.1(67.9^{+2.2}_{-2.0})$	$67.16 \pm 0.87(67.2^{+1.7}_{-1.7})$
σ_8	$0.62 \pm 0.16(0.62^{+0.29}_{-0.29})$	$0.796 \pm 0.019(0.796^{+0.038}_{-0.038})$	$0.778 \pm 0.018(0.778^{+0.034}_{-0.034})$	$0.797 \pm 0.020(0.797^{+0.037}_{-0.040})$	$0.779 \pm 0.017(0.779^{+0.032}_{-0.032})$

TABLE III. *Neutrinos:* Mean values for some of the most relevant cosmological parameters in this study, together with their 68% (95%) CL errors for the some of the possible data combinations here considered, based on the baseline ACT-DR6 plus Planck lensing datasets. Upper bounds are quoted at 95% CL significance.

Parameter	Full lensing	Full lensing + BAO	Full lensing + BAO + DES	Full lensing + BAO + SN	Full lensing + BAO + DES + SN
$\sum m_\nu$[eV]	<1.42	<0.527	<0.664	<0.490	<0.606
$\Omega_{\rm m}$	$0.55^{+0.13}_{-0.15}(0.55^{+0.29}_{-0.27})$	$0.320 \pm 0.010(0.320^{+0.023}_{-0.022})$	$0.316 \pm 0.011(0.316^{+0.024}_{-0.023})$	$0.3173 \pm 0.0094(0.317^{+0.021}_{-0.020})$	$0.3130 \pm 0.0097(0.313^{+0.021}_{-0.020})$
H_0	$55.2^{+5.5}_{-6.2}(55^{+10}_{-10})$	$67.90 \pm 0.73(67.9^{+1.4}_{-1.4})$	$68.29 \pm 0.71(68.3^{+1.4}_{-1.4})$	$68.07 \pm 0.72(68.1^{+1.4}_{-1.5})$	$68.38 \pm 0.71(68.4^{+1.4}_{-1.4})$
σ_8	$0.689 \pm 0.053(0.69^{+0.11}_{-0.11})$	$0.796 \pm 0.017(0.796^{+0.035}_{-0.036})$	$0.776 \pm 0.017(0.776^{+0.036}_{-0.037})$	$0.798 \pm 0.016(0.798^{+0.033}_{-0.034})$	$0.779 \pm 0.016(0.779^{+0.033}_{-0.034})$

as it does not rely on a large number of datasets and relies only on large scale and CMB lensing observables. When adding further lensing observations from galaxy surveys such as the one considered along this manuscript (DES), the limit is further strengthened to 0.77 eV. Nevertheless DES measurements are not very effective when constraining neutrino masses because they prefer a lower value of the clustering parameter σ_8, which is anticorrelated with the neutrino mass as can be clearly noticed from the contours illustrated in Fig. 1. Indeed, notice that, while the value of σ_8 from the combination of ACT-DR6 and BAO remains unchanged when adding Supernova Ia observations to the data analyses, it diminishes (very mildly though) if DES measurements are those included in the

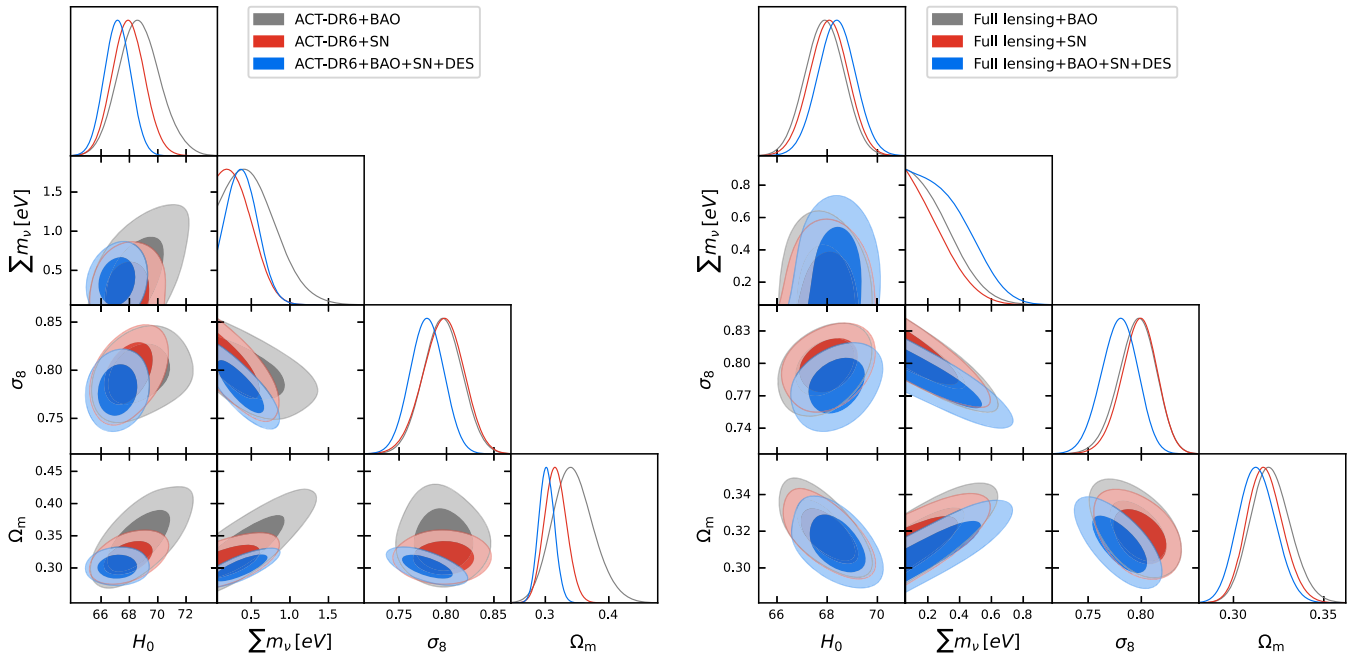

FIG. 1. *Neutrinos:* Left (right) panel: One-dimensional posterior probability distributions and two-dimensional 68% and 95% CL allowed contours for $\sum m_a$, H_0, $\Omega_{\rm m}$ and σ_8 from combinations of the baseline ACT-DR6 (ACT-DR6 plus Planck lensing) with other low-redshift observables considered along this work.

combined fit. In this regard, SNIa data is more efficient constraining the neutrino mass, and a 95% CL limit of 0.72 eV is obtained from the combination of ACT-DR6, BAO, and SN data. Notice also from Table II that the σ_8 anomaly is absent, as we are only dealing with CMB lensing data and not with CMB temperature observations, which are those driving this tension. This result will remain unchanged in the following sections. Table III shows the impact of the addition of Planck lensing measurements to the baseline ACT-DR6 data. Notice first of all that the neutrino mass constraints are notably improved. Also, compared to the results of Planck, the limit $\sum m_\nu <$ 0.60 eV obtained from the combination of Planck lensing plus BAO and acoustic scale priors quoted in Ref. [85] tightens to $\sum m_\nu < 0.49$ eV for ACT-DR6, Planck lensing, BAO, and SN priors. This constraint loosens when considering DES observations, due to the lower value of σ_8 preferred by the former dataset and its anticorrelation with $\sum m_\nu$. Concerning the Hubble parameter, the value is always slightly higher than that inferred from CMB temperature anisotropies and therefore the Hubble tension is slightly alleviated. All the constraints shown in Table III are illustrated in Fig. 1 (right panel), which shows the posterior probability distributions and the two-dimensional 68% and 95% CL allowed contours. A very interesting aspect to notice from this figure is the change in the direction of the degeneracy line between $\Omega_{\rm m}$ and H_0 when Planck CMB lensing information is added to the baseline ACT-DR6 dataset, as we can see by comparing the difference in the contours in the (H_0, $\Omega_{\rm m}$) plane between the left and right panels of Fig. 1. The reason for that is due to the fact that CMB lensing and BAO constraints on the former plane are almost orthogonal [74]. In the case of CMB lensing $\Omega_{\rm m}$ and H_0 are anticorrelated, providing ACT-DR6 lensing data the following constraint on the three-dimensional $\sigma_8 - H_0$–$\Omega_{\rm m}$ plane [75]:

$$\left(\frac{\sigma_8}{0.3}\right)\left(\frac{\Omega_{\rm m}}{0.3}\right)^{0.23}\left(\frac{\Omega_{\rm m}h^2}{0.13}\right)^{-0.32} = 0.994 \pm 0.020, \quad (1)$$

where the error refers to 68% CL. This linelike degeneracy translates into a narrow region in the σ_8–$\Omega_{\rm m}$ with

$$\sigma_8\Omega_{\rm m}^{0.25} = 0.606 \pm 0.016, \quad (2)$$

with 68% CL error. Planck lensing measurements also provide a constraint on a narrow band in the three-dimensional $\sigma_8 - H_0$–$\Omega_{\rm m}$ parameter space [85],

$$\left(\frac{\sigma_8}{0.3}\right)\left(\frac{\Omega_{\rm m}}{0.3}\right)^{0.23}\left(\frac{\Omega_{\rm m}h^2}{0.13}\right)^{-0.32} = 0.986 \pm 0.020, \quad (3)$$

with 68% CL error. The corresponding band in the σ_8–$\Omega_{\rm m}$ plane in this case is given by [85]

$$\sigma_8\Omega_{\rm m}^{0.25} = 0.589 \pm 0.020, \quad (4)$$

with, again, 68% CL uncertainty. In the case of BAO instead, $\Omega_{\rm m}$ and H_0 are positively correlated. Since the BAO constraint dominates that of ACT-DR6, when these two datasets are combined the resulting denegeracy line in the (H_0, $\Omega_{\rm m}$) plane follows the trend of the BAO-only contours. However, when considering also Planck CMB lensing measurements the combination of ACT-DR6 with those makes CMB lensing more powerful than BAO observations, following now the degeneracy line in the (H_0, $\Omega_{\rm m}$) plane the CMB lensing one, rather than the one from BAO observations.

B. Constraints on axions

The constraints on massive axions, fixing the neutrino mass to 0.06 eV, are shown in Table IV and V and in Fig. 2. Notice that the results when only ACT-DR6 lensing measurements are considered are very similar to those previously presented for the massive neutrino case, except for a small difference. In the axion case, the addition of DES observations to ACT-DR6 and BAO measurements results in a stronger axion mass bound than that found when SNIa luminosity distance data are considered. The limit is $m_a < 1.28$ eV ($m_a < 1.46$ eV) at 95% CL for the combination of ACT-DR6 plus BAO plus DES (ACT-DR6 plus BAO plus SN). When adding Planck lensing information, the limits on the axion mass are only improved when a few data sets (e.g., lensing plus BAO) are involved, while they are only mildly better for the cases in which a larger sample of observations are analysed. For instance, from the combination of ACT-DR6 plus BAO plus SN the 95% CL upper bound on the axion mass changes from 1.46 eV to 1.2 eV when adding Planck lensing data. As can be noticed from Fig. 2 also for this case, as in the massive neutrino one, there is a change in the direction of the degeneracy line between $\Omega_{\rm m}$ and H_0 when Planck CMB lensing information is added to the baseline ACT-DR6 dataset. The values of the Hubble constant are also always slightly higher than those obtained in the canonical ΛCDM scenario with Planck temperature anisotropies; for the combination of ACT-DR6 plus BAO, we obtain $H_0 = 70.2 \pm 1.7$, which is much closer to the value measured by local probes, $H_0 = 73.04 \pm 1.04$ km/s/Mpc [91], lowering considerably the statistical significance of the so-called Hubble constant tension. A similar argument applies to almost all the remaining cases when considering ACT-DR6 plus Planck lensing data combined.

C. Joint constraints on axions and neutrinos

The constraints on a mixed dark matter scenario are summarized in Table VI, VII, and Fig. 3. We notice that the limits on both the neutrino and the axion masses shown in Table VI, even if close to those obtained in

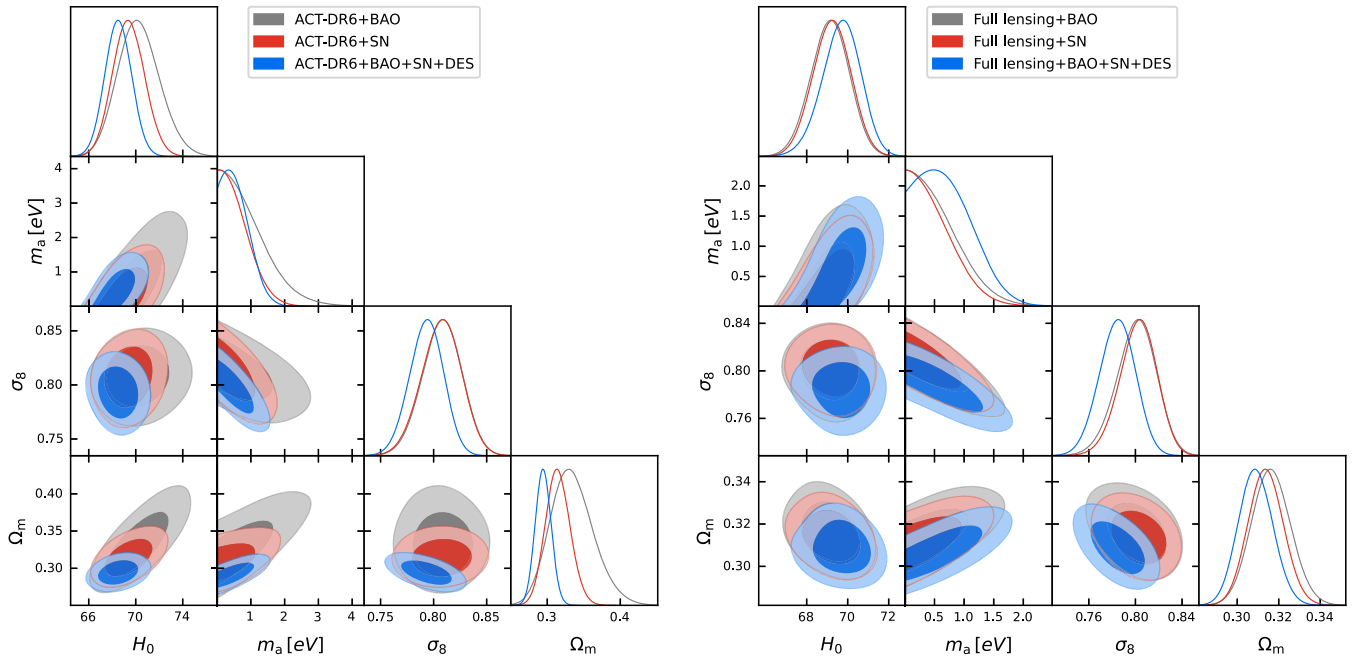

FIG. 2. *Axion:* Left (right) panel: One-dimensional posterior probability distributions and two-dimensional 68% and 95% CL allowed contours for m_a, H_0, Ω_m and σ_8 from combinations of the baseline ACT-DR6 (ACT-DR6 plus Planck lensing) with other low-redshift observables considered along this work.

the neutrino-only and axion-only hot dark matter scenarios (see Table II and IV), are more constraining, due to the fact that the hot dark matter energy density is now shared among two different species and therefore the amount of each of them is reduced with respect to the case in which only one of them is present. The very same argument applies when considering also Planck lensing measurements in the data analyses. The tightest 95% CL limits we find here are $\sum m_\nu < 0.43$ eV and $m_a < 1.11$ eV for the combination of CMB lensing data, BAO, and SN observations.When compared to the tightest cosmological limits quoted in the literature,

TABLE IV. *Axion:* Mean values for some of the most relevant cosmological parameters in this study, together with their 68% (95%) CL errors for the some of the possible data combinations here considered, based on the baseline ACT-DR6 dataset. Upper bounds are quoted at 95% CL significance.

Parameter	ACT-DR6	ACT-DR6 + BAO	ACT-DR6 + BAO + DES	ACT-DR6 + BAO + SN	ACT-DR6 + BAO + DES + SN
m_a[eV]	<3.11	<2.19	<1.28	<1.46	<1.27
Ω_m	$0.86^{+0.49}_{-1.1}(<2.86)$	$0.333^{+0.028}_{-0.032}(0.333^{+0.061}_{-0.057})$	$0.293 \pm 0.011(0.293^{+0.023}_{-0.023})$	$0.314 \pm 0.016(0.314^{+0.033}_{-0.030})$	$0.294 \pm 0.010(0.294^{+0.020}_{-0.019})$
H_0	56^{+20}_{-20} (unc)	$70.2 \pm 1.7(70.2^{+3.6}_{-3.5})$	$68.5 \pm 1.1(68.5^{+2.1}_{-2.0})$	$69.4 \pm 1.3(69.4^{+2.6}_{-2.4})$	$68.5 \pm 1.1(68.5^{+2.1}_{-2.0})$
σ_8	$0.70^{+0.17}_{-0.15}(0.70^{+0.31}_{-0.33})$	$0.808 \pm 0.017(0.808^{+0.037}_{-0.037})$	$0.793 \pm 0.015(0.793^{+0.028}_{-0.031})$	$0.807 \pm 0.018(0.807^{+0.037}_{-0.038})$	$0.793 \pm 0.015(0.793^{+0.028}_{-0.030})$

TABLE V. *Axion:* Mean values for some of the most relevant cosmological parameters in this study, together with their 68% (95%) CL errors for the some of the possible data combinations here considered, based on the baseline ACT-DR6 plus Planck-lensing datasets. Upper bounds are quoted at 95% CL significance.

Parameter	Full lensing	Full lensing + BAO	Full lensing + BAO + DES	Full lensing + BAO + SN	Full lensing + BAO + DES + SN
m_a[eV]	<1.79	<1.34	<1.61	<1.20	<1.47
Ω_m	$0.382 \pm 0.049(0.382^{+0.10}_{-0.096})$	$0.3163 \pm 0.0088(0.316^{+0.019}_{-0.019})$	$0.3102 \pm 0.0085(0.310^{+0.018}_{-0.018})$	$0.3138 \pm 0.0080(0.314^{+0.016}_{-0.015})$	$0.3089 \pm 0.0078(0.309^{+0.016}_{-0.014})$
H_0	$63.4^{+3.7}_{-4.4}(63^{+8}_{-8})$	$69.14 \pm 0.88(69.1^{+1.7}_{-1.8})$	$69.68 \pm 0.87(69.7^{+1.8}_{-1.9})$	$69.23 \pm 0.87(69.2^{+1.7}_{-1.7})$	$69.70 \pm 0.88(69.7^{+1.8}_{-1.9})$
σ_8	$0.762 \pm 0.031(0.762^{+0.060}_{-0.061})$	$0.801 \pm 0.016(0.801^{+0.033}_{-0.035})$	$0.783 \pm 0.015(0.783^{+0.031}_{-0.032})$	$0.803 \pm 0.015(0.803^{+0.031}_{-0.032})$	$0.784 \pm 0.014(0.784^{+0.027}_{-0.029})$

TABLE VI. *Axion and Neutrinos:* Mean values for some of the most relevant cosmological parameters in this study, together with their 68% (95%) CL errors for the some of the possible data combinations here considered, based on the baseline ACT-DR6 lensing dataset. Upper bounds are quoted at 95% CL significance.

Parameter	ACT-DR6	ACT-DR6 + BAO	ACT-DR6 + BAO + DES	ACT-DR6 + BAO + SN	ACT-DR6 + BAO + DES + SN
m_a[eV]	<4.06	<1.86	<1.07	<1.19	<1.08
$\sum m_\nu$[eV]	<3.67	<1.14	<0.732	<0.654	<0.684
Ω_m	$1.7^{+1.1}_{-2.1}$(unc)	$0.359 \pm 0.033(0.359^{+0.073}_{-0.069})$	$0.306 \pm 0.013(0.306^{+0.027}_{-0.025})$	$0.320 \pm 0.016(0.320^{+0.035}_{-0.034})$	$0.305 \pm 0.012(0.305^{+0.025}_{-0.024})$
H_0	< 55.5(unc)	$70.6 \pm 1.8(70.6^{+3.8}_{-3.7})$	$68.3 \pm 1.0(68.3^{+2.0}_{-1.9})$	$69.1 \pm 1.2(69.1^{+2.7}_{-2.6})$	$68.3 \pm 1.0(68.3^{+2.1}_{-2.0})$
σ_8	$0.57 \pm 0.16(0.57^{+0.35}_{-0.34})$	$0.792 \pm 0.019(0.792^{+0.037}_{-0.038})$	$0.774 \pm 0.017(0.774^{+0.033}_{-0.034})$	$0.792 \pm 0.020(0.792^{+0.037}_{-0.038})$	$0.775 \pm 0.017(0.775^{+0.032}_{-0.032})$

TABLE VII. *Axion and Neutrinos:* Mean values for some of the most relevant cosmological parameters in this study, together with their 68% (95%) CL errors for the some of the possible data combinations here considered, based on the baseline ACT-DR6 plus Planck lensing datasets. Upper bounds are quoted at 95% CL significance.

Parameter	Full lensing	Full lensing + BAO	Full lensing + BAO + DES	Full lensing + BAO + SN	Full lensing + BAO + DES + SN
m_a[eV]	<1.79	<1.23	<1.38	<1.11	<1.32
$\sum m_\nu$[eV]	<1.32	<0.492	<0.583	<0.432	<0.533
Ω_m	$0.56^{+0.12}_{-0.14}(0.56^{+0.28}_{-0.26})$	$0.324 \pm 0.010(0.324^{+0.022}_{-0.022})$	$0.319 \pm 0.010(0.319^{+0.022}_{-0.021})$	$0.3191 \pm 0.0090(0.319^{+0.018}_{-0.017})$	$0.3154 \pm 0.0091(0.315^{+0.018}_{-0.017})$
H_0	$55.8 \pm 5.0(56^{+10}_{-10})$	$69.01 \pm 0.86(69.0^{+1.7}_{-1.7})$	$69.51 \pm 0.85(69.5^{+1.8}_{-1.8})$	$69.17 \pm 0.85(69.2^{+1.7}_{-1.7})$	$69.61 \pm 0.83(69.6^{+1.6}_{-1.7})$
σ_8	$0.682 \pm 0.047(0.682^{+0.091}_{-0.087})$	$0.789 \pm 0.018(0.789^{+0.033}_{-0.036})$	$0.770 \pm 0.016(0.770^{+0.033}_{-0.032})$	$0.792 \pm 0.017(0.792^{+0.035}_{-0.036})$	$0.774 \pm 0.015(0.774^{+0.029}_{-0.031})$

the former constraints may seem not highly competitive, but they are impressively robust and independent, as they do not rely on CMB temperature and polarization anisotropies; they are based on low-redshift phenomena as lensing and large scale structure data. As in the previous cases, within this mixed hot dark matter scenario the Hubble constant tension is also relieved, i.e., the significance is much smaller than in the standard ΛCDM case. In some cases, it does not neither reach the 2.5σ significance level.

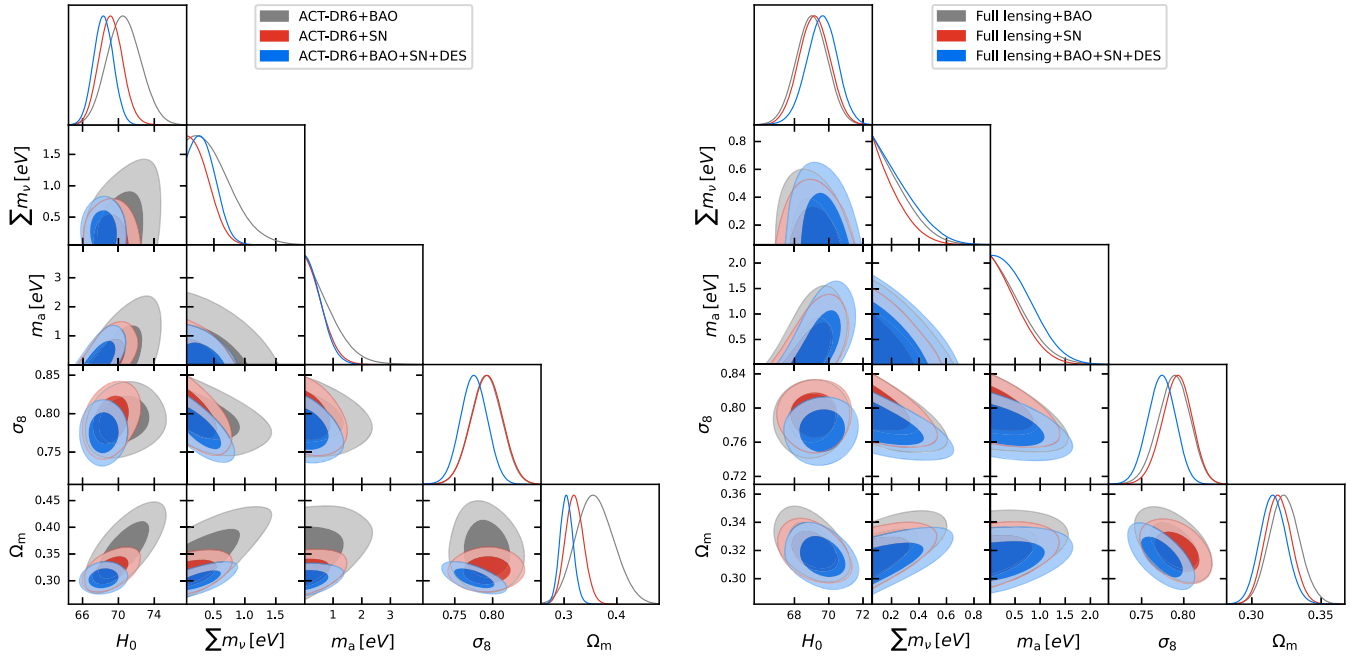

FIG. 3. *Axion and Neutrinos:* Left (right) panel: One-dimensional posterior probability distributions and two-dimensional 68% and 95% CL allowed contours for $\sum m_\nu$, m_a, H_0, Ω_m, and σ_8 from combinations of the baseline ACT-DR6 (ACT-DR6 plus Planck lensing) with other low-redshift observables considered along this work.

IV. CONCLUSIONS

Low-redshift phenomena play a highly relevant role in cosmology nowadays. Lensing of the cosmic microwave background photons and of large scale structure by intervening galaxies, as well as large-scale structure standard rulers (BAO) have been shown to improve the bounds on a variety of cosmological parameters derived from Planck CMB temperature and polarization anisotropies. Very well-known examples are the neutrino and the axion masses and abundances. The constraining power of cosmological observations is much more efficient when these low-redshift observations are included in the data analyses. However, a pending question is how robust would be the limits that these low-redhsift probes impose by themselves, without relying in the CMB temperature input. Here we have explored such a situation, finding very competitive limits, much superior than those found in current laboratory searches for thermal relic properties. The tightest bounds we find for the neutrino and axion masses are $\sum m_\nu < 0.43$ eV and $m_a < 1.1$ eV at 95% CL respectively, for the Full lensing + BAO + SN dataset combination.

These limits reassess both the robustness and the constraining power of cosmological thermal relic searches. For instance, in the neutrino case, the limits inferred by current beta-decay experiments such as KATRIN impose that $\sum m_\nu \lesssim 2.0$ eV [92], while the bounds on the effective Majorana neutrino mass from neutrinoless double beta-decay experiments set the bound $\sum m_\nu \lesssim 0.1$–2.0 eV [93], both at 90% CL.

Intriguingly, also when discarding CMB temperature and polarization anistropies in the data analyses, long-standing tensions such as the Hubble constant and the clustering parameter σ_8 ones are either much less significant or completely absent. Future lensing measurements from CMB and/or galaxy surveys may have the key to resolve these pending issues.

ACKNOWLEDGMENTS

This work has been supported by the Spanish MCIN/AEI/10.13039/501100011033 Grant No. PID2020–113644GB-I00 (RH and OM) and by the European ITN project HIDDeN (No. H2020-MSCA-ITN-2019/860881-HIDDeN) and SE project ASYMMETRY (HORIZON-MSCA-2021-SE-01/101086085-ASYMMETRY) and well as by the Generalitat Valenciana Grants No. PROMETEO/2019/083 and No. CIPROM/2022/69. E. D. V. is supported by a Royal Society Dorothy Hodgkin Research Fellowship. This article is based upon work from COST Action No. CA21136 addressing observational tensions in cosmology with systematics and fundamental physics (CosmoVerse) supported by COST (European Cooperation in Science and Technology). We acknowledge IT Services at The University of Sheffield for the provision of services for High Performance Computing.

[1] R. D. Peccei and H. R. Quinn, Phys. Rev. Lett. **38**, 1440 (1977).
[2] R. D. Peccei and H. R. Quinn, Phys. Rev. D **16**, 1791 (1977).
[3] F. Wilczek, Phys. Rev. Lett. **40**, 279 (1978).
[4] S. Weinberg, Phys. Rev. Lett. **40**, 223 (1978).
[5] J. Preskill, M. B. Wise, and F. Wilczek, Phys. Lett. **120B**, 127 (1983).
[6] L. F. Abbott and P. Sikivie, Phys. Lett. B **120B**, 133 (1983).
[7] M. Dine and W. Fischler, Phys. Lett. **120B**, 137 (1983).
[8] C. A. Baker *et al.*, Phys. Rev. Lett. **97**, 131801 (2006).
[9] J. M. Pendlebury *et al.*, Phys. Rev. D **92**, 092003 (2015).
[10] C. Abel *et al.*, Phys. Rev. Lett. **124**, 081803 (2020).
[11] T. W. B. Kibble, J. Phys. A **9**, 1387 (1976).
[12] A. Vilenkin, Phys. Rev. D **24**, 2082 (1981).
[13] T. W. B. Kibble, G. Lazarides, and Q. Shafi, Phys. Rev. D **26**, 435 (1982).
[14] P. Sikivie, Phys. Rev. Lett. **48**, 1156 (1982).
[15] A. Vilenkin and A. E. Everett, Phys. Rev. Lett. **48**, 1867 (1982).
[16] A. D. Linde, Phys. Lett. **158B**, 375 (1985).
[17] M. C. Huang and P. Sikivie, Phys. Rev. D **32**, 1560 (1985).
[18] D. Seckel and M. S. Turner, Phys. Rev. D **32**, 3178 (1985).
[19] R. L. Davis, Phys. Lett. B **180**, 225 (1986).
[20] D. H. Lyth, Phys. Lett. B **236**, 408 (1990).
[21] A. D. Linde and D. H. Lyth, Phys. Lett. B **246**, 353 (1990).
[22] A. Vilenkin and E. P. S. Shellard, *Cosmic Strings and Other Topological Defects* (Cambridge University Press, Cambridge, England, 2000).
[23] M. S. Turner, Phys. Rev. Lett. **59**, 2489 (1987); **60**, 1101(E) (1988).
[24] Z. G. Berezhiani, A. S. Sakharov, and M. Y. Khlopov, Sov. J. Nucl. Phys. **55**, 1063 (1992).
[25] C. Brust, D. E. Kaplan, and M. T. Walters, J. High Energy Phys. 12 (2013) 058.
[26] D. Baumann, D. Green, and B. Wallisch, Phys. Rev. Lett. **117**, 171301 (2016).
[27] F. D'Eramo, R. Z. Ferreira, A. Notari, and J. L. Bernal, J. Cosmol. Astropart. Phys. 11 (2018) 014.
[28] F. Arias-Aragón, F. D'Eramo, R. Z. Ferreira, L. Merlo, and A. Notari, J. Cosmol. Astropart. Phys. 11 (2020) 025.
[29] F. Arias-Aragón, F. D'Eramo, R. Z. Ferreira, L. Merlo, and A. Notari, J. Cosmol. Astropart. Phys. 03 (2021) 090.
[30] D. Green, Y. Guo, and B. Wallisch, J. Cosmol. Astropart. Phys. 02 (2022) 019.
[31] F. D'Eramo and S. Yun, Phys. Rev. D **105**, 075002 (2022).
[32] L. Di Luzio, M. Giannotti, E. Nardi, and L. Visinelli, Phys. Rep. **870**, 1 (2020).

[33] S. Hannestad, A. Mirizzi, and G. Raffelt, J. Cosmol. Astropart. Phys. 07 (2005) 002.
[34] A. Melchiorri, O. Mena, and A. Slosar, Phys. Rev. D **76**, 041303 (2007).
[35] S. Hannestad, A. Mirizzi, G. G. Raffelt, and Y. Y. Y. Wong, J. Cosmol. Astropart. Phys. 08 (2007) 015.
[36] S. Hannestad, A. Mirizzi, G. G. Raffelt, and Y. Y. Y. Wong, J. Cosmol. Astropart. Phys. 04 (2008) 019.
[37] S. Hannestad, A. Mirizzi, G. G. Raffelt, and Y. Y. Y. Wong, J. Cosmol. Astropart. Phys. 08 (2010) 001.
[38] M. Archidiacono, S. Hannestad, A. Mirizzi, G. Raffelt, and Y. Y. Y. Wong, J. Cosmol. Astropart. Phys. 10 (2013) 020.
[39] E. Giusarma, E. Di Valentino, M. Lattanzi, A. Melchiorri, and O. Mena, Phys. Rev. D **90**, 043507 (2014).
[40] E. Di Valentino, S. Gariazzo, E. Giusarma, and O. Mena, Phys. Rev. D **91**, 123505 (2015).
[41] E. Di Valentino, E. Giusarma, M. Lattanzi, O. Mena, A. Melchiorri, and J. Silk, Phys. Lett. B **752**, 182 (2016).
[42] M. Archidiacono, T. Basse, J. Hamann, S. Hannestad, G. Raffelt, and Y. Y. Y. Wong, J. Cosmol. Astropart. Phys. 05 (2015) 050.
[43] F. D'Eramo, F. Hajkarim, and S. Yun, Phys. Rev. Lett. **128**, 152001 (2022).
[44] F. D'Eramo, F. Hajkarim, and S. Yun, J. High Energy Phys. 10 (2021) 224.
[45] E. Di Valentino, S. Gariazzo, and O. Mena, Phys. Rev. D **104**, 083504 (2021).
[46] N. Palanque-Delabrouille, C. Yèche, N. Schöneberg, J. Lesgourgues, M. Walther, S. Chabanier, and E. Armengaud, J. Cosmol. Astropart. Phys. 04 (2020) 038.
[47] E. di Valentino, S. Gariazzo, and O. Mena, Phys. Rev. D **106**, 043540 (2022).
[48] W. Giarè, E. Di Valentino, A. Melchiorri, and O. Mena, Mon. Not. R. Astron. Soc. **505**, 2703 (2021).
[49] W. Giarè, F. Renzi, A. Melchiorri, O. Mena, and E. Di Valentino, Mon. Not. R. Astron. Soc. **511**, 1373 (2022).
[50] F. D'Eramo, E. Di Valentino, W. Giarè, F. Hajkarim, A. Melchiorri, O. Mena, F. Renzi, and S. Yun, J. Cosmol. Astropart. Phys. 09 (2022) 022.
[51] A. Notari, F. Rompineve, and G. Villadoro, Phys. Rev. Lett. **131**, 011004 (2023).
[52] E. Di Valentino, S. Gariazzo, W. Giarè, A. Melchiorri, O. Mena, and F. Renzi, arXiv:2212.11926.
[53] P. F. de Salas, D. V. Forero, S. Gariazzo, P. Martínez-Miravé, O. Mena, C. A. Ternes, M. Tórtola, and J. W. F. Valle, J. High Energy Phys. 02 (2021) 071.
[54] I. Esteban, M. C. Gonzalez-Garcia, M. Maltoni, T. Schwetz, and A. Zhou, J. High Energy Phys. 09 (2020) 178.
[55] F. Capozzi, E. Di Valentino, E. Lisi, A. Marrone, A. Melchiorri, and A. Palazzo, Phys. Rev. D **104**, 083031 (2021).
[56] J. R. Bond, G. Efstathiou, and M. Tegmark, Mon. Not. R. Astron. Soc. **291**, L33 (1997).
[57] M. Zaldarriaga, D. N. Spergel, and U. Seljak, Astrophys. J. **488**, 1 (1997).
[58] G. Efstathiou and J. R. Bond, Mon. Not. R. Astron. Soc. **304**, 75 (1999).
[59] S. Aiola *et al.* (ACT Collaboration), J. Cosmol. Astropart. Phys. 12 (2020) 047.
[60] D. Dutcher *et al.* (SPT-3G Collaboration), Phys. Rev. D **104**, 022003 (2021).
[61] E. Di Valentino, W. Giarè, A. Melchiorri, and J. Silk, Phys. Rev. D **106**, 103506 (2022).
[62] E. Di Valentino, S. Gariazzo, W. Giarè, and O. Mena, arXiv:2305.12989.
[63] E. Di Valentino and A. Melchiorri, Astrophys. J. Lett. **931**, L18 (2022).
[64] W. Handley and P. Lemos, Phys. Rev. D **103**, 063529 (2021).
[65] W. Giarè, F. Renzi, O. Mena, E. Di Valentino, and A. Melchiorri, Mon. Not. R. Astron. Soc. **521**, 2911 (2023).
[66] E. Di Valentino, W. Giarè, A. Melchiorri, and J. Silk, Mon. Not. R. Astron. Soc. **520**, 210 (2023).
[67] M. Forconi, W. Giarè, E. Di Valentino, and A. Melchiorri, Phys. Rev. D **104**, 103528 (2021).
[68] W. Giarè, S. Pan, E. Di Valentino, W. Yang, J. de Haro, and A. Melchiorri, arXiv:2305.15378.
[69] J. C. Hill *et al.*, Phys. Rev. D **105**, 123536 (2022).
[70] V. Poulin, T. L. Smith, and A. Bartlett, Phys. Rev. D **104**, 123550 (2021).
[71] P. A. R. Ade *et al.* (Planck Collaboration), Astron. Astrophys. **571**, A16 (2014).
[72] M. Kaplinghat, L. Knox, and Y.-S. Song, Phys. Rev. Lett. **91**, 241301 (2003).
[73] J. Lesgourgues, L. Perotto, S. Pastor, and M. Piat, Phys. Rev. D **73**, 045021 (2006).
[74] M. S. Madhavacheril *et al.* (ACT Collaboration), arXiv:2304.05203.
[75] F. J. Qu *et al.* (ACT Collaboration), arXiv:2304.05202.
[76] A. Lewis, A. Challinor, and A. Lasenby, Astrophys. J. **538**, 473 (2000).
[77] C. Howlett, A. Lewis, A. Hall, and A. Challinor, J. Cosmol. Astropart. Phys. 04 (2012) 027.
[78] L. Caloni, M. Gerbino, M. Lattanzi, and L. Visinelli, J. Cosmol. Astropart. Phys. 09 (2022) 021.
[79] L. Di Luzio, G. Martinelli, and G. Piazza, Phys. Rev. Lett. **126**, 241801 (2021).
[80] L. Di Luzio, C. Martin, M. Jorge, O. Guido, A. José, and G. Piazza, Phys. Rev. D **108**, 035025 (2023).
[81] J. E. Kim, Phys. Rev. Lett. **43**, 103 (1979).
[82] M. A. Shifman, A. I. Vainshtein, and V. I. Zakharov, Nucl. Phys. **B166**, 493 (1980).
[83] J. Torrado and A. Lewis, arXiv:2005.05290.
[84] A. Gelman and D. B. Rubin, Stat. Sci. **7**, 457 (1992).
[85] N. Aghanim *et al.* (Planck Collaboration), Astron. Astrophys. **641**, A8 (2020).
[86] K. S. Dawson *et al.* (BOSS Collaboration), Astron. J. **145**, 10 (2013).
[87] S. Alam *et al.* (BOSS Collaboration), Mon. Not. R. Astron. Soc. **470**, 2617 (2017).
[88] S. Alam *et al.* (eBOSS Collaboration), Phys. Rev. D **103**, 083533 (2021).
[89] D. M. Scolnic *et al.* (Pan-STARRS1 Collaboration), Astrophys. J. **859**, 101 (2018).
[90] T. M. C. Abbott *et al.* (DES Collaboration), Phys. Rev. D **98**, 043526 (2018).
[91] A. G. Riess *et al.*, Astrophys. J. Lett. **934**, L7 (2022).
[92] M. Aker *et al.* (KATRIN Collaboration), Nat. Phys. **18**, 160 (2022).
[93] S. Abe *et al.* (KamLAND-Zen Collaboration), Phys. Rev. Lett. **130**, 051801 (2023).